Linear elastic fracture mechanics approach to edge debonding in plated beams

CCC 2008 - Challenges for Civil Construction
Torres Marques et al. (Eds)

LINEAR ELASTIC FRACTURE MECHANICS APPROACH TO EDGE DEBONDING IN PLATED BEAMS

A. Carpinteri[*], L. De Lorenzis[†], M. Paggi[*], G. Zavarise[†]

[*] Department of Structural and Geotechnical Engineering
Politecnico di Torino
C.so Duca degli Abruzzi 24, 10129 Torino, Italy
e-mail: alberto.carpinteri@polito.it, marco.paggi@polito.it

[†] Department of Innovation Engineering
University of Salento
Via per Monteroni, 73100 Lecce, Italy
e-mail: laura.delorenzis@unile.it, giorgio.zavarise@unile.it

Keywords: Edge debonding, Fracture mechanics, FRP reinforcement, Numerical modelling, Snap-back instability.

Summary: *In this paper a simple linear elastic fracture mechanics approach is proposed for prediction of edge debonding in plated beams. The analytical model results in simple equations, suitable for immediate design use. The load–deflection curve of a plated beam, from the onset of debonding up to the complete separation of the plate, is obtained by controlling the length of the interfacial debonding crack. Its shape clearly shows that snap-back or snap-through instabilities may arise when the beam is loaded under displacement or force control. Analytical predictions are also compared with finite element results based on an interfacial cohesive crack model. It is shown that predictions of the proposed analytical model match very closely the numerical solution, provided that an effective crack length accounting for the size of the fracture process zone is used in the calculations.*

1 INTRODUCTION

Plate bonding is an effective and cost-efficient technique to increase the load-bearing capacity and/or the stiffness of existing beams. In the past decade, fiber-reinforced polymer (FRP) composite plates have almost totally replaced the more traditional steel plates for this application. Among the possible failure modes of plate bonded beams, several mechanisms related to debonding of the plate from the substrate have been identified by previous researches. Due to the brittle and unstable character of such failures, their prediction has been the subject of several investigations. In particular, this paper focuses on the so-called “edge debonding” mechanism, whereby failure occurs by the formation and rapid growth of an interfacial crack between the edge of the plate and the beam.

A detailed review of existing models for prediction of edge debonding failures is available in [1]. Most of the models reviewed therein adopt a stress-based criterion for failure prediction. Rabinovitch and Frostig [2] proposed a fracture-mechanics based approach, where the higher-order theory is used for the stress analysis of the plated beam, and the J-integral formulation is adopted for the evaluation of the energy release rate. In the attempt to simplify the formulation, Rabinovitch [3] adopted the virtual crack extension method coupled with different stress analysis models, including: (i) the two- and one-parameter elastic foundation models for the evaluation of the interfacial stresses between the plate and the substrate, (ii) the equivalent beam model, (iii) the finite element analysis. By comparing results with those obtained from the application of the higher-order theory, he showed that the virtual crack extension method using the stress results of the elastic foundation models provides an acceptable estimate of the energy release rate.

In the most recent studies on edge debonding, fracture mechanics based approaches are becoming increasingly established [4, 5]. Carpinteri et al. [5] used three-dimensional finite element modelling to analyze edge debonding in beams with non-rectangular cross-section, assuming a linear behaviour for the materials and a non-linear interfacial cohesive law for the plate-substrate interface. Their results show that, when the bending stiffness of the plated beam is considerably higher than that of the unplated beam, snap-back instabilities may take place.

In this paper, a simple linear elastic fracture mechanics approach is proposed for the prediction of edge debonding in plated beams. This approach is analogous to the equivalent beam model adopted by Rabinovitch [3] and aims at simplifying more detailed models based on the elastic foundation theory [6, 7]. In this paper, useful closed-form equations to estimate the critical load for the onset of edge debonding are determined. Moreover, the analysis is extended to the determination of the entire load–deflection curve of the beam, obtained according to a *crack length control scheme*, as first proposed by Carpinteri [8, 9] and then recently generalized [10] to interface mechanical problems. The shape of the obtained curve delivers interesting information on the beam behaviour following the whole process of edge debonding, and on the role played by the most significant design variables. Finally, analytical predictions are compared with the results of a nonlinear finite element model. This model assumes linearly elastic behaviour for the materials, but considers a nonlinear interface cohesive law taking into account Mixed Mode effects [11]. Predictions provided by the analytical model are expected to deviate quite significantly from those obtained on the basis of a more sophisticated approach, in accordance with previous results [3]. However, it will be shown that a suitably enhanced version of such a simple model can be devised to match more closely the numerical solution.

2 ANALYTICAL MODEL

2.1 Assumptions

The model considers a plated beam of length l (Figure 1), supported with a hinge at one end and a roller at the other end, and loaded with a point load F at the mid-span.

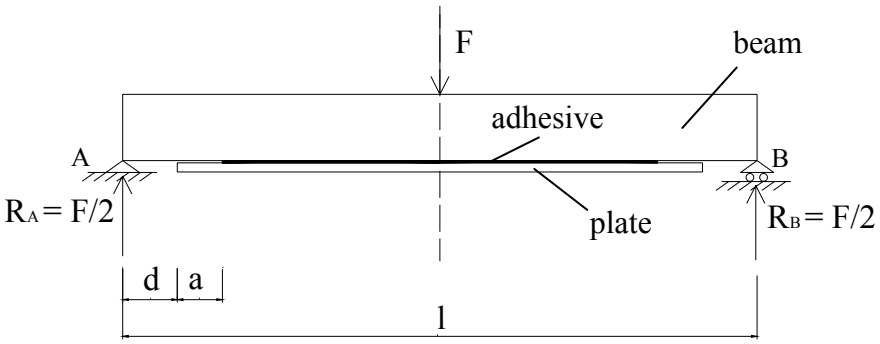

Figure 1: Plated beam under a mid-span force.

The model is based on the following assumptions:

- plane cross-sections remain plane for both the unstrengthened (unplated) and the strengthened (plated) portions of the beam;
- beam and plate materials are assumed to be linear elastic;
- the bending stiffnesses of the unstrengthened and strengthened cross-sections are indicated as EI_u and EI_s, respectively. The gradual development of composite action between the beam and the strengthening plate is neglected, assuming that all sections in presence of a bonded plate have stiffness EI_s. This corresponds to assuming an infinite stiffness of the p_T -

g_T relationship, p_T and g_T being the interfacial shear stress and tangential relative displacement, respectively;

- the interfacial crack of length a develops symmetrically on both sides of the beam and propagates always in the same direction. In other words, the crack is assumed to propagate in pure Mode II conditions, i.e. Mixed Mode effects are neglected. For the sake of simplicity, Figure 1 shows that the crack forms in the adhesive. Its actual path follows the weakest link between the substrate, the adhesive, the interface between substrate and adhesive, and the interface between adhesive and plate.

2.2 Mid-span deflection and compliance

The mid-span deflection of the beam under three-point bending can be expressed as follows

$$v = F\left[\frac{l^3}{48EI_s} + \frac{(d+a)^3}{6}\left(\frac{1}{EI_u} - \frac{1}{EI_s}\right)\right] \tag{1}$$

where d is the distance between the support and the cutoff section of the strengthening plate, and a is the length of the interfacial crack. Hence, the compliance C is a function of a, which can be expressed as

$$C(a) = \frac{l^3}{48EI_s} + \frac{(d+a)^3}{6}\left(\frac{1}{EI_u} - \frac{1}{EI_s}\right) \tag{2}$$

As it is reasonable to expect, the compliance increases with the length of the interfacial crack. Considering that

$$0 \le a \le \frac{l}{2} - d \tag{3}$$

it follows that the compliance varies between a minimum value, C_{min}, and a maximum value, C_{max}, given by

$$C_{min} = C(0) = \frac{l^3}{48EI_s} + \frac{d^3}{6}\left(\frac{1}{EI_u} - \frac{1}{EI_s}\right) \tag{4a}$$

$$C_{max} = C\left(\frac{l}{2} - d\right) = \frac{l^3}{48EI_u} \tag{4b}$$

where C_{max} corresponds to the compliance of the unplated beam.

2.3 Energy release rate and conditions for crack propagation

Under load control, the energy release rate is given by

$$G = \frac{F^2}{4b_f}\left.\frac{dC}{da}\right|_F \tag{5}$$

where b_f is the width of the plate. Combining Eqs. (2) and (5) yields

$$G = \frac{F^2}{8b_f}(d+a)^2\left(\frac{1}{EI_u}-\frac{1}{EI_s}\right) \tag{6}$$

The value of the applied load leading to crack propagation in presence of an interfacial crack of length a, $F_{cr}(a)$, can be obtained by equating the energy release rate given by Eq. (6) to its critical value, G_{cr}. Note that, following the assumptions of the model, this critical value corresponds to the interfacial fracture energy in Mode II. The resulting expression for the critical load is

$$F_{cr}(a) = \sqrt{\frac{8b_f G_{cr}}{(d+a)^2\left(\frac{1}{EI_u}-\frac{1}{EI_s}\right)}} \tag{7}$$

In particular, if the initial crack length is equal to zero, we have

$$F_{cr}(0) = \sqrt{\frac{8b_f G_{cr}}{d^2\left(\frac{1}{EI_u}-\frac{1}{EI_s}\right)}} \tag{8}$$

Under displacement control, the energy release rate is given by

$$G = \frac{v^2}{4C^2 b_f}\left.\frac{dC}{da}\right|_v \tag{9}$$

which yields

$$G = \frac{v^2}{8b_f}\frac{(d+a)^2\left(\frac{1}{EI_u}-\frac{1}{EI_s}\right)}{\left[\frac{l^3}{48EI_s}+\frac{(d+a)^3}{6}\left(\frac{1}{EI_u}-\frac{1}{EI_s}\right)\right]^2} \tag{10}$$

Eq. (10) can also be obtained by combining Eqs. (1) and (6). The value of the applied mid-span

deflection leading to crack propagation in presence of an interfacial crack of length a, $v_{cr}(a)$, can be obtained by equating the energy release rate given by Eq. (10) to its critical value, G_{cr}. It can also be expressed as follows

$$v_{cr}(a) = C(a)F_{cr}(a) \tag{11}$$

where $C(a)$ and $F_{cr}(a)$ are given by Eqs. (2) and (7), respectively. In particular, if the initial crack length is equal to zero, we have

$$v_{cr}(0) = C(0)F_{cr}(0) \tag{12}$$

2.4 Dimensionless formulation

It is now assumed that the beam cross-section is rectangular, of width b and depth h, that the plate has thickness t, and that E and E_s are, respectively, the elastic moduli of the beam material and of the strengthening plate. All the dimensionless variables introduced as follows are illustrated in Table 1.

Table 1: Definition of dimensionless variables.

Definition	Description
$\bar{F}_{cr} = \dfrac{F_{cr}}{b_f\sqrt{EG_{cr}h}}$	Dimensionless force
$\bar{a} = \dfrac{a}{l}$	Dimensionless crack length
$\bar{d} = \dfrac{d}{l}$	Dimensionless distance between the support and the cutoff section of the strengthening plate
$\bar{h} = \dfrac{h}{l}$	Dimensionless beam depth
$\bar{b}_f = \dfrac{b_f}{b}$	Dimensionless plate width
$k = \dfrac{EI_s}{EI_u}$	Bending stiffness ratio between plated and unplated cross-sections
$n = \dfrac{E_s}{E}$	Modular ratio between plate and beam materials
$\bar{t} = \dfrac{t}{h}$	Dimensionless plate thickness
$\bar{v} = \dfrac{v}{l}$	Dimensionless mid-span displacement
$\bar{C} = C\dfrac{b_f\sqrt{EG_{cr}h}}{l}$	Dimensionless compliance
$\bar{G}_{cr} = \dfrac{G_{cr}}{Eh}$	Dimensionless Mode II fracture energy

Elastic analysis of the cross-section easily shows that, in the particular case of $\bar{b}_f = 1$, the bending stiffness ratio between plated and unplated cross-sections can be obtained as

$$k = \frac{n^2\bar{t}^4 + 4n\bar{t}^3 + 6n\bar{t}^2 + 4n\bar{t} + 1}{n\bar{t} + 1} \tag{13}$$

With simple manipulations, Eq. (7) can be cast in dimensionless form as follows

$$\bar{F}_{cr}\left(\bar{a}\right) = \sqrt{\frac{2}{3}\frac{\bar{h}^2}{\bar{b}_f\left(\bar{a}+\bar{d}\right)^2}\frac{k}{k-1}} \tag{14}$$

and Eq. (2) in dimensionless form becomes

$$\bar{C}\left(\bar{a}\right) = \frac{\bar{b}_f\sqrt{\bar{G}_{cr}}}{4k\bar{h}^2}\left[1 + 8\left(k-1\right)\left(\bar{a}+\bar{d}\right)^3\right] \tag{15}$$

Finally, the following dimensionless version of Eq. (11) holds

$$\bar{v}_{cr}(\bar{a}) = \bar{C}(\bar{a})\bar{F}_{cr}(\bar{a}) \tag{16}$$

where $\bar{v}_{cr}$ is the critical value of the dimensionless mid-span deflection.

2.5 Load-deflection response using the crack length control scheme

Assuming that the initial length of the interfacial crack is zero, no propagation occurs until $F_{cr}(0)$ and $v_{cr}(0)$ (given by Eqs. (8) and (12), respectively) are simultaneously reached. In this stage, the load-deflection response of the beam is linear with compliance given by Eq. (4a). The subsequent load-displacement response can be obtained by combining $F_{cr}(a)$ and $v_{cr}(a)$ given by Eqs. (7) and (11), or, using the dimensionless form, by combining $\bar{F}_{cr}\left(\bar{a}\right)$ and $\bar{v}_{cr}(\bar{a})$ given by Eqs. (14) and (16). The dimensionless load-deflection curve is shown in Figure 2 for different values of k, and for realistic values of the remaining dimensionless variables, namely: $\bar{b}_f = 1$, $\bar{h} = 0.12$, $\bar{d} = 0.125$, $\bar{G}_{cr} = 1.81\times10^{-8}$. The thick straight line corresponds to the load-deflection behaviour of the unplated beam. It is evident that the curves feature both snap-back and snap-through instabilities, i.e. discontinuities appear if the process is either displacement- or load-controlled [12]. The predicted behaviour is thus very similar to that obtained by Carpinteri et al. [5, 13] by finite element modelling and by Carpinteri et al. [12] using a one-parameter elastic foundation model for the plate-substrate interface. It is also worth noting that, for smaller values of the stiffness ratio k, the critical dimensionless load is higher, although the unstable snap-back branch is sharper.

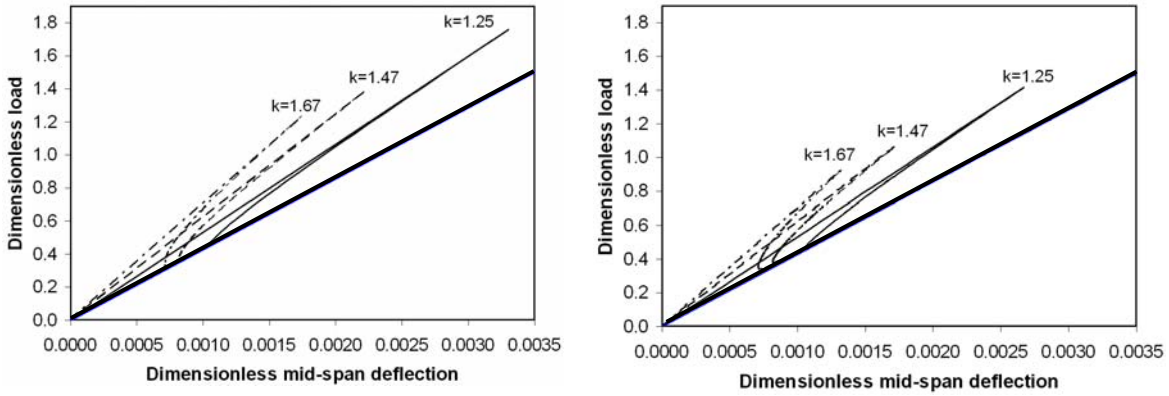

(a) Analytical predictions (b) Numerical predictions

Figure 2: Dimensionless load vs. mid-span deflection curves.

Among the available test results, those presented by Buyukozturk et al. [14] can be used for a qualitative comparison with the previous analytical predictions. In such tests, beams with FRP strengthening plates of different lengths were considered. From a theoretical standpoint, this process is equivalent to adopting the interfacial crack length as the controlling parameter of the test. The experimental load vs. mid-span deflection curves are shown in Figure 3, where the different curves correspond to beams with different FRP lengths. As the figure clearly shows, the ideal curve joining the peaks of the various experimental load vs. mid-span deflection curves reproduces the snap-back profile predicted by the analytical model. Obviously, the pre-peak stage of the curve features a nonlinear behaviour which is not included in the model.

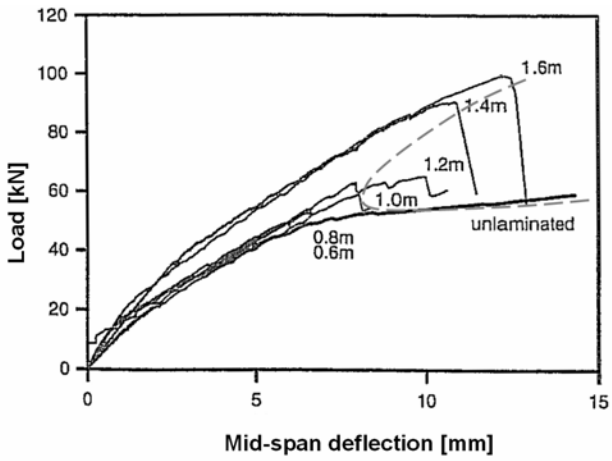

Figure 3: Experimental load vs. mid-span deflection curves for the tested beams considered in [14].

3 FINITE ELEMENT MODEL

In the two-dimensional finite element (FE) model of the plated beam adopted herein, plane stress eight-node finite elements are used for the discretization of the continuum. As the study mainly focuses on the onset and stability of the edge debonding process, and in accordance with the assumptions of the analytical model, the beam and plate materials are both assumed to behave linear elastically and only the nonlinear behaviour of the interface is retained in the model.

The plate-substrate interface is modelled with zero-thickness interface elements. The mechanical behaviour of such elements is usually described by suitable interface constitutive laws, where the

equivalent nodal forces transmitted along the interface are related to the displacement discontinuities in the corresponding directions (see also [15] for a detailed overview of mathematical methods for interface constitutive laws).

The plate-substrate interface in the problem under examination is subjected to both shear and normal stresses, hence interfacial constitutive laws have to be assumed in both directions. For a review of different possible approaches in cohesive zone modelling of Mixed Mode fracture problems, see [16]. For a plated beam, the effect of Mode Mixity caused by bending effects has not yet been clarified by the previous research.

In the present paper, coupled cohesive laws derived from a potential are considered in the normal and tangential directions. With this approach, the fracture energy is the same in all mode mixities. Tension relates the normal relative displacement, $g_N > 0$, to the normal stress, p_N, while shear relates the tangential relative displacement, g_T, to the tangential stress, p_T. Frequently used coupled cohesive laws derived from a potential are those developed in [17] and [18]. Both use a dimensionless coupling parameter between the normal and tangential laws. The present study adopts a simplified version of the laws in [18], where the constant branch of the curves is taken of zero length. Hence, the cohesive laws implemented herein are bilinear. This simple shape is able to capture the three characteristic parameters of the interface, i.e. the fracture energies (areas underneath the curves), the cohesive strengths, $p_{N\,max}$ and $p_{T\,max}$, and the linear elastic properties (slopes of the curves in the ascending branch). For this reason the bilinear model is often used to model the interfacial behaviour of FRP bonded to quasi-brittle substrates [19].

The normal and shear cohesive laws are coupled by introducing a measure of interface opening and sliding, λ, as follows

$$\lambda = \sqrt{\left(\frac{g_N}{g_{Nc}}\right)^2 + \left(\frac{g_T}{g_{Tc}}\right)^2} \tag{17}$$

where g_{Nc} and g_{Tc} are, respectively, the normal and shear relative displacements at peak traction. The normal and tangential tractions, F_N and F_T, are computed as functions of the normal and tangential relative displacements using the following relationships

$$F_N = \begin{cases} \dfrac{p_{N\,max}}{\lambda_{max}} \dfrac{g_N}{g_{Nc}} & 0 < \lambda \le \lambda_{max} \\ \dfrac{p_{N\,max}}{\lambda} \dfrac{1-\lambda}{1-\lambda_{max}} \dfrac{g_N}{g_{Nc}} & \lambda_{max} < \lambda < 1 \end{cases} \tag{18a}$$

$$F_T = \begin{cases} \dfrac{p_{N\,max}}{\lambda_{max}} \dfrac{g_{Nc}}{g_{Tc}} \dfrac{g_T}{g_{Tc}} & 0 < \lambda \le \lambda_{max} \\ \dfrac{p_{N\,max}}{\lambda} \dfrac{1-\lambda}{1-\lambda_{max}} \dfrac{g_{Nc}}{g_{Tc}} \dfrac{g_T}{g_{Tc}} & \lambda_{max} < \lambda < 1 \end{cases} \tag{18b}$$

Note that only one cohesive strength is explicitly defined ($p_{N\,max}$), as the normal and tangential laws are derived from a potential. The curves vary with the coupling parameter λ. The parameter λ_{max} has no specific influence on the numerical results. It is chosen sufficiently small as compared to

the unity, to obtain a stiff ascending branch of the cohesive laws, which agrees with the experimental observations on the FRP-concrete interfacial behavior.

The crack-length control scheme is used in order to follow the whole range of load-deflection behaviour of the plated beam, from the onset of debonding to the complete detachment of the plate. Such numerical scheme was proposed by Carpinteri [8, 9] for the analysis of the unstable mechanical response of quasi-brittle materials, and then extended in [10] to interface crack problems. Applications of this method to the problem of FRP debonding can be found in [11].

4 NUMERICAL EXAMPLE

The example considers a beam characterized by the geometrical and mechanical parameters reported in Table 2. The total fracture energy is kept equal to 65 N/m, whereas the maximum normal traction is equal to $p_{N\max} = 6$ MPa. The comparison between analytical predictions and numerical results is proposed in Figure 2 in terms of dimensionless load vs. dimensionless mid-span deflection. The comparison between Figures 2a and 2b shows that the analytical model overestimates the critical (peak) load corresponding to the onset of FRP debonding, if compared to the FE solution. This agrees with previous results [3], and is expectable, when considering the high degree of approximation involved in the analytical model. In particular, the analytical model does not incorporate the detailed distribution of interfacial stresses at the crack tip and the size of the fracture process zone. Conversely, these aspects are taken into account by the numerical model.

Table 2: Parameters used in the numerical simulations.

Parameter	Case 1	Case 2	Case 3
Dimensional parameters			
l [m]	1	1	1
d [m]	0.125	0.125	0.125
h [m]	0.12	0.12	0.12
b [m]	0.1	0.1	0.1
b_f [m]	0.1	0.1	0.1
E [GPa]	30	30	30
E_s [GPa]	210	210	210
t [m]	0.0015	0.0030	0.0045
G_{cr} [N/m]	65	65	65
Dimensionless parameters			
$\bar{d}$	0.125	0.125	0.125
$\bar{h}$	0.12	0.12	0.12
$\bar{b_f}$	1	1	1
$\bar{t}$	0.0250	0.0125	0.0375
n	7.0	7.0	7.0
k	1.25	1.47	1.67
$\bar{G}_{cr}$	1.81E−8	1.81E−8	1.81E−8

In order to better interpret the discrepancy between analytical and numerical solutions, Figure 4 shows the dimensionless load vs. the relative length of the interfacial crack, $2a/l$. The diagram refers to the parameters corresponding to Case 2 in Table 2, but considers $\bar{d} = 0.05$ instead of $\bar{d} = 0.125$ in

order to follow a broader range of the curve. Also in this plot the analytical curve is seen to overestimate the numerical predictions. However, if the analytical model is applied by considering an increased fictitious crack length, $a + \Delta a$, instead of the real crack length a, the resulting analytical curve matches closely the numerical one. In this example, the value of Δa yielding the best agreement between analytical and numerical results is equal to approximately 40 mm. This corresponds to the length of the fracture process zone in front of the crack tip. Such a length has been estimated from the interfacial stress distributions given by the FE solution model, and appears approximately constant during the entire debonding process. If the dimensionless load vs. dimensionless mid-span deflection curve is evaluated by using the incremented crack length $a + \Delta a$ (Figure 5), a very close match between analytical and numerical results is achieved, the maximum deviation being about 4%. This can be clearly observed by comparing Figure 5 with Figure 2b. Note that this approach shows analogies with the so-called "point method", widely used in the study of fatigue crack propagation, as well as with the effective crack approach used to account for small scale yielding in linear elastic fracture mechanics.

4 CONCLUSIONS

A simple linear elastic fracture mechanics approach for prediction of edge debonding in plated beams has been presented in this paper. Closed-form equations have been provided, through which an approximate estimate of the critical load for the onset of edge debonding can be obtained under the simplifying assumptions of the model. Moreover, the analysis has been extended to the determination of the entire load-deflection curve of the beam, obtained by controlling the length of the interfacial debonding crack. The shape of the curve shows that snap-back or snap-through instabilities may arise when the beam is loaded under displacement or force control. As the stiffness ratio between the plated and the unplated cross-sections decreases, the critical dimensionless load increases but the unstable snap-back branch becomes sharper.

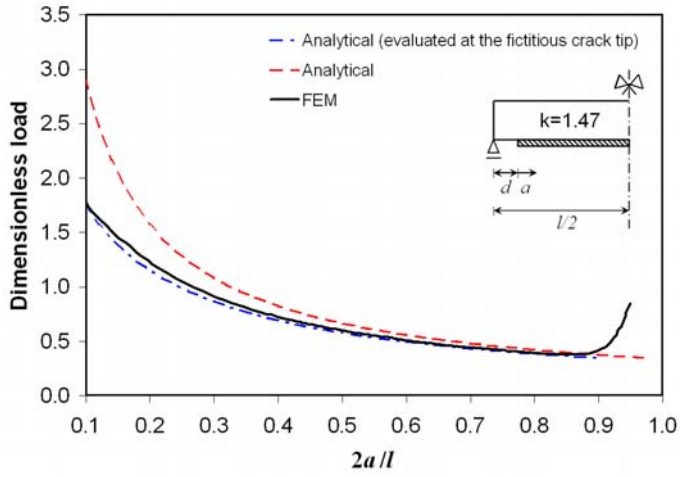

Figure 4: Dimensionless load vs. dimensionless interface crack length.

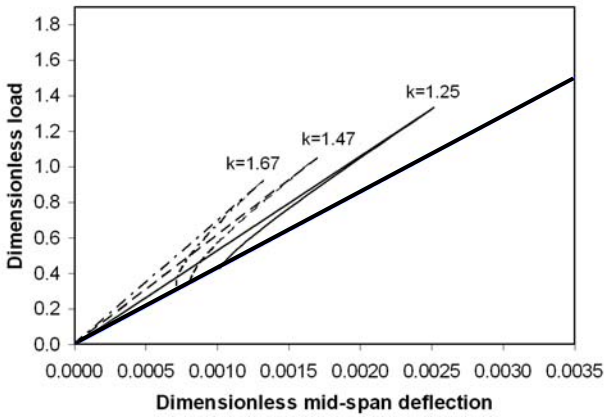

Figure 5: Analytical predictions using $\Delta a = 40\ mm$.

Analytical predictions have been compared with results of finite element modelling. It has been shown that the proposed analytical model significantly overestimates the critical load, due to its simplifying assumptions including infinite stiffness of the interfacial traction-separation law. However, analytical predictions match very closely the numerical solution, provided that an effective crack length $a + \Delta a$ accounting for the size of the fracture process zone is used in the calculations. This approach shows analogies with the so-called "point method", widely used in the study of fatigue crack propagation, as well as with the effective crack approach used to account for small scale yielding in linear elastic fracture mechanics. Further research is needed to evaluate Δa theoretically, and to further validate the conclusions of the present study on a wider range of cases.

REFERENCES

[1] Smith, S., and Teng, J.G., "FRP-strengthened RC beams. I: review of debonding strength models", *Engineering Structures*, 24(4): 385-395 (2002).

[2] Rabinovitch, O., and Frostig, Y., "Non-linear high-order analysis of cracked RC beams externally strengthened with FRP strips", ASCE *Journal of Structural Engineering*, 127(4): 381-389 (2001).

[3] Rabinovitch, O., "Fracture-mechanics failure criteria for RC beams strengthened with FRP strips – a simplified approach", *Composite Structures*, 64: 479-492 (2004).

[4] Colombi, P., "Reinforcement delamination of metallic beams strengthened by FRP strips: fracture mechanics based approach", *Engineering Fracture Mechanics*, 73: 1980-1995 (2006).

[5] Carpinteri, A., Lacidogna, G. and Paggi, M., "Acoustic emission monitoring and numerical modelling of FRP delamination in RC beams with non-rectangular cross-section", RILEM *Materials & Structures*, 40: 553-566 (2007).

[6] Carpinteri, A, Cornetti, P. and Pugno, N., "Debonding in FRP strengthened beams: stress assessment versus fracture mechanics approach", In: *Design, Assessment and Retrofitting of RC Structures*, Vol. 2 of the Proceedings of the 6th Conference on Fracture Mechanics of Concrete and Concrete Structures (FraMCoS), Catania, Italy, Taylor & Francis (GBR), 6th Fracture Mechanics of Concrete and Concrete Structures (FraMCoS), Catania, Italy June 17-22, 2007, 1053-1060 (2007).

[7] Cornetti, P., Puzzi, S., Carpinteri, A., "Failure mechanisms in beams strengthened with adhesive strips", Proceedings of the XVIII AIMETA Conference, Brescia, Italy, on CD-ROM (2007).

[8] Carpinteri, A., "Interpretation of the Griffith instability as a bifurcation of the global equilibrium", in S. Shah (ed.), Application of fracture mechanics to cementitious composites (Proc. of a NATO Advanced Research Workshop, Evanston, USA, 1984), 287-316 Martinus Nijhoff Publishers, Dordrecht (1985).

[9] Carpinteri, A., "Cusp catastrophe interpretation of fracture instability", *Journal of the Mechanics and Physics of Solids*, 37: 567-582 (1989).

[10] Carpinteri, A., Paggi, M. and Zavarise, G., "Snap-back instability in micro-structured composites and its connection with superplasticity", *Strength, Fracture and Complexity*, 3: 61-72 (2005).

[11] Carpinteri, A., Paggi, M., "Analysis of snap-back instability in the delamination of FRP-strengthened beams", *ASCE Journal of Engineering Mechanics*, submitted (2008).

[12] Carpinteri, A., Cornetti, P., Lacidogna, G., and Paggi, M., "A unified approach for the analysis of failure modes in FRP-retrofitted concrete beams", *Advances in Structural Engineering*, submitted (2008).

[13] Carpinteri, A., Lacidogna, G. and Paggi, M., "On the competition between delamination and shear failure in retrofitted concrete beams and related scale effects", In: *Design, Assessment and Retrofitting of RC Structures*, Vol. 2 of the Proceedings of the 6th Conference on Fracture Mechanics of Concrete and Concrete Structures (FraMCoS), Catania, Italy, Taylor & Francis (GBR), 6th Fracture Mechanics of Concrete and Concrete Structures (FraMCoS), Catania, Italy June 17-22, 2007, 1069-1076, (2007).

[14] Buyukozturk, O., Leung, C., Hearing, B. and Gunes, O., "Delamination criterion for concrete beams retrofitted with FRP laminates", In H. Mihashi and K. Rokugo (Eds.), Fracture Mechanics of Concrete Structures, Proceedings of FraMCoS-3, AEDIFICATIO Publishers, Freiburg, Germany, 1771-1782 (1998).

[15] Paggi, M., Carpinteri, A., and Zavarise, G., "A unified interface constitutive law for the study of fracture and contact problems in heterogeneous materials", in: P. Wriggers, U. Nackenhorst (eds.), *Analysis and simulation of contact problems*, Lecture notes in applied and computational mechanics, 27: 297-304, 2006. Springer-Verlag, Berlin (2006).

[16] De Lorenzis, L., and Zavarise, G., "Modeling of mixed-mode debonding in the peel test applied to superficial reinforcements", to appear (2008).

[17] Tvergaard, V., "Effect of fiber debonding in a whisker-reinforced metal". *Materials Science and Engineering*, A, 125: 203-213 (1990).

[18] Tvergaard, V., Hutchinson, J.W., "The relation between crack growth resistance and fracture process parameters in elastic-plastic solids." *Journal of the Mechanics and Physics of Solids*, 40: 1377-1397 (1992).

[19] Yuan, H., Teng, J.G., Seracino, R., Wu, Z.S., and Yao, J., "Full-range behaviour of FRP-to-concrete bonded joints", *Engineering Structures*, 26: 553-565 (2004).